International Journal of Pharmaceutics 426 (2012) 170–181

Contents lists available at SciVerse ScienceDirect

International Journal of Pharmaceutics

journal homepage: www.elsevier.com/locate/ijpharm

Pharmaceutical nanotechnology

PEG/RGD-modified magnetic polymeric liposomes for controlled drug release and tumor cell targeting

Wenya Su[a,b,1], Hanjie Wang[a,b,1], Sheng Wang[a,b], Zhenyu Liao[a,b], Shiyin Kang[a,b], Yao Peng[a,b], Lei Han[c,*], Jin Chang[a,b,**]

[a] Institute of Nanobiotechnology, School of Materials Science and Engineering, Tianjin University, Tianjin 300072, PR China
[b] Tianjin Key Laboratory of Composites and Functional Materials, Tianjin 300072, PR China
[c] Department of Neurosurgery, Laboratory of Neuro-Oncology, Tianjin Medical University General Hospital, Tianjin 300052, PR China

ARTICLE INFO

Article history:
Received 9 October 2011
Received in revised form
15 December 2011
Accepted 7 January 2012
Available online 14 January 2012

Keywords:
Drug delivery
Polymeric liposomes
Magnetic nanoparticles
Tumor Targeting
RGD peptide

ABSTRACT

Polymeric liposomes (PEG/RGD-MPLs), composed of amphiphilic polymer octadecyl-quaternized modified poly (γ-glutamic acid) (OQPGA), PEGylated OQPGA, RGD peptide grafted OQPGA and magnetic nanoparticles, was prepared successfully. These PEG/RGD-MPLs could be used as a multifunctional platform for targeted drug delivery. The results showed that PEG/RGD-MPLs were multilamellar spheres with nano-size (50–70 nm) and positive surface charge (28–42 mV). Compared with magnetic conventional liposomes (MCLs), PEG/RGD-MPLs exhibited sufficient size and zeta potential stability, low initial burst release and less magnetic nanoparticles leakage. The cell uptake results suggested that the PEG/RGD-MPLs (with RGD and magnetic particles) exhibited more drug cellular uptake than non RGD and non magnetism carriers in MCF-7 cells. MTT assay revealed that PEG/RGD-MPLs showed lower in vitro cytotoxicity to GES-1 cells at ≤100 μg/mL. These data indicated that the multifunctional PEG/RGD-MPLs may be an alternative formulation for drug delivery system.

1. Introduction

Currently, a critical challenge in developing drug delivery system was how to achieve an optimal pharmacokinetic profile to allow sufficient targeting and avoid rapid clearance by the reticuloendothelial system (RES) simultaneously. Many studies have been done on developing drug delivery systems in order to achieve long-circulation (Xiong et al., 2005). Huang and Li have developed PEGylated liposome by surface incorporation of polyethylene glycol (PEG) in liposome to minimize the clearance by the RES and prolong circulation time of liposome (Li and Huang, 2009; Klibanov et al., 1990; Blume and Cevc, 1990; Maruyama et al., 1991; Allen et al., 1991; Maeda et al., 2000). Various efforts have been undertaken to enable drug to accumulate in target tumor sites, among which magnetic drug targeting (MDT) and receptor-specific targeting were developed. Using paramagnetic particles as drug carriers, MDT can guide their accumulation in target tissues under strong local magnetic fields, and has been applied in the treatment of cancer patients with some success (Lubbe et al., 2001; Ito et al., 2006; Hirao et al., 2003). As conventional paramagnetic nanoparticles, superparamagnetic ferroferric oxide (Fe_3O_4) was encapsulated in nanocarriers for magnetic separation and magnetic tissue targeting (Benyettou et al., 2009). Another mechanism used in drug targeting involves receptor-specific targeting which takes advantage of over-expressed surface receptors on tumor cells. Receptor-targeted nanocarriers can be used to load drugs thereby facilitating delivery of high drug payloads to tumors. Meanwhile, nanocarriers can protect non-target normal organs from the toxic drug effects (Gabizon et al., 1982; Park et al., 2005; Zhang et al., 2010a,b). Recently, RGD (arginine–glycine–aspartic acid)-modified liposomes have been developed as drug delivery system. The RGD sequence was known to serve as a recognition motif for integrin $\alpha\nu\beta3$ over-expressed on tumor cells surface, which enhanced the opportunities of liposomes binding to tumor cells (Xiong et al., 2005; Ruoslahti, 1996).

It has become the hotspot in nowadays studies that how to construct an effective delivery nanocarriers with sufficient stability. Self-assembled liposomes were used as a delivery system combining receptor-specific targeting and magnetic targeting (Zhu et al., 2010). However, liposomes were prone to adhere to each other and fuse to form larger vesicles in suspension, which restrict its

* Corresponding author. Tel.: +86 022 60362662; fax: +86 022 60362662.
** Corresponding author at: Institute of Nanobiotechnology, School of Materials Science and Engineering, Tianjin University, Tianjin 300072, PR China. Tel.: +86 022 27401821; fax: +86 022 27401821.
E-mail addresses: superhanlei@hotmail.com (L. Han), jinchang@tju.edu.cn (J. Chang).
[1] Both authors contributed equally to this work.

0378-5173/$ – see front matter © 2012 Elsevier B.V. All rights reserved.
doi:10.1016/j.ijpharm.2012.01.013

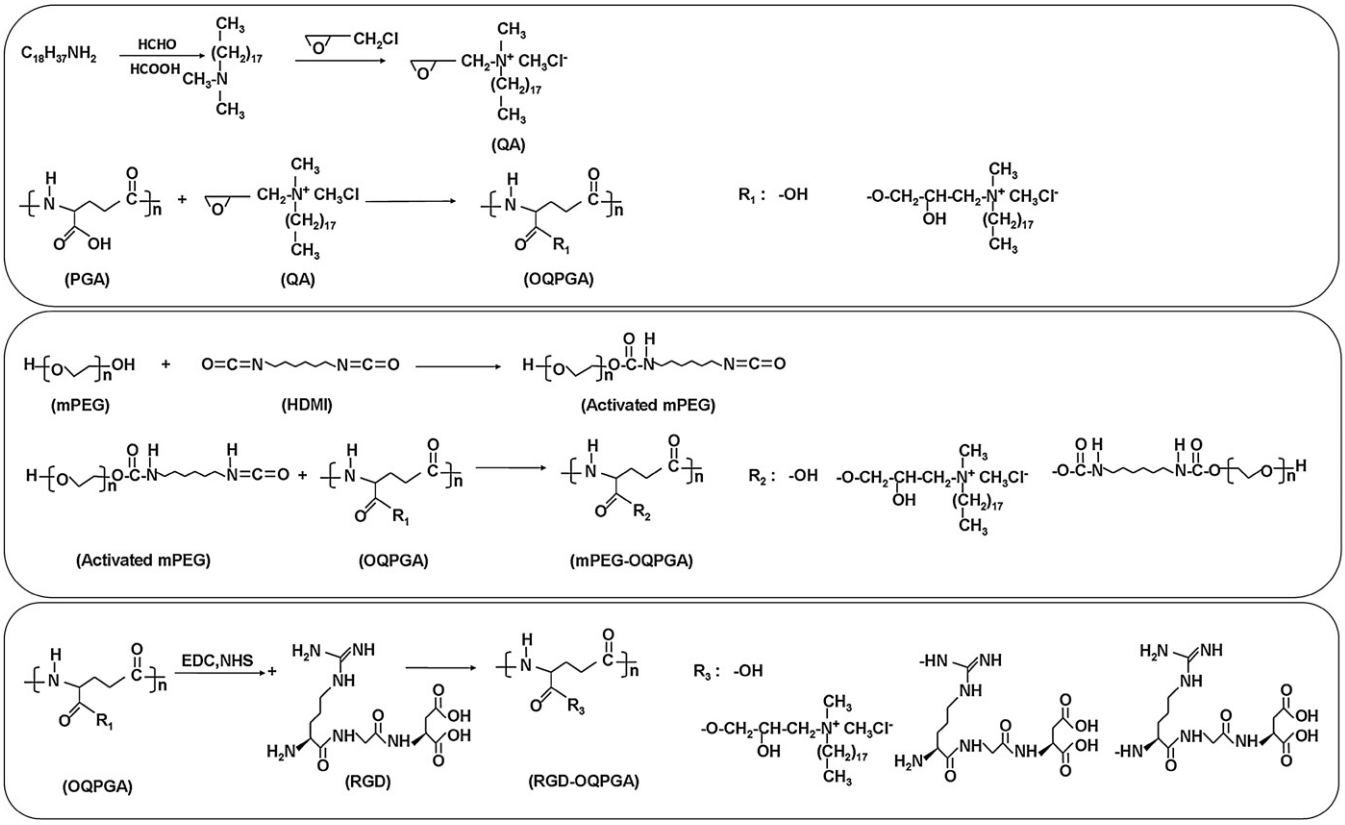

Fig. 1. Schematic illustration of the synthetic processes of QA, OQPGA, mPEG-OQPGA and RGD-OQPGA.

application in therapy (Zhang and Granick, 2006). Toward this end, many efforts have been made to design a sufficiently stable drug delivery nanocarrier. Among various nanocarriers, polymeric liposomes (PLs) showed promising ability because of good physical and thermal stability, excellent solubility in water, and high effectiveness in drug encapsulation (Liang et al., 2008a,b). For the past several years, PLs were self-assembled by amphiphilic polymers base on chitosan derivatives in our lab with some success. Chitosan is a natural cationic polymer which has been under investigation for various biomedical and pharmaceutical applications. However, its poor aqueous solubility is major drawbacks for its use at physiological conditions (Verheul et al., 2008). In this case, our lab developed hydrophilic carboxymethyl chitosan (CMC) (Liang et al., 2008a,b) and lysine modified chitosan (LCS) (Wang et al., 2010) successfully in past years. The synthetic routes were so complicated that the repeatability of experiments decreased and the cost of production enhanced.

In this study, a new amphiphilic polymer octadecyl-quaternized modified poly (γ-glutamic acid) (OQPGA) were synthesized by poly-γ-glutamic acid (PGA) and octadecyl dimethylammonium chloride (QA). PGA was water-soluble, biocompatibility, biodegradable and non-toxicity (Prencipe et al., 2009). We simplified the experimental procedures and improved the repeatability of experiments after PGA has been substituted for chitosan derivatives (CMC and LCS). In order to construct a sufficiently stable tumor targeting delivery system combining tumor accumulating and enhanced intracellular delivery, polymeric liposomes (PEG/RGD-MPLs) were developed by OQPGA, mPEG modified OQPGA (mPEG-OQPGA), RGD modified OQPGA (RGD-OQPGA) and magnetic nanoparticles. Their particle size, zeta potential, morphology and magnetic characterization were studied. To research its drug release effect, epidoxorubicin (EPI) as a model drug was encapsulated into the PEG/RGD-MPLs. The influences of samples/MCF-7 cells incubation time on cellular uptake were investigated. The cell-viability test of GES-1 cells was assessed by MTT assay.

2. Materials and methods

2.1. Materials

PGA with a molecular weight (MW) of 5×10^4 was supplied by Guilin peptide Technology Limited (Guangxi, China). RGD peptide of the arginine–glycine–aspartic acid sequence was obtained by GL Biochem (Shanghai) Ltd. N-(3-dimethylaminopropyl)-N-ethylcarbodiimide hydrochloride (EDC·HCl) and N-hydroxysuccinimide (NHS) were obtained from DingguoBiotechnology Co. Ltd. (Shanghai, China). mPEG with a molecular weight (MW) of 2×10^3 was purchased from Aldrich. Pyrene was purchased from Sigma–Aldrich. EPI and Chol were supplied by Tianjin People's pharmaceutical factory (Tianjin, China). The MCF-7 cells and GES-1 cells were supplied by Tianjin Medical University General Hospital (Tianjin, China). Fe_3O_4 nanoparticles were synthesized by the method described by Sun and Zeng (2002). All other chemicals were reagent grade and were used as received.

2.2. Synthesis of OQPGA, PEG-OQPGA and RGD-OQPGA

Octadecyl dimethylammonium chloride (QA) was synthesized as reported in our previous work (Fig. 1) (Liang et al., 2008a,b). The general preparation of OQPGA according to the literature report (Blank et al., 2002) was shown in Fig. 1: typically, 2 g of PGA powder was dissolved in 160 mL isopropanol (IPA), followed by addition of 10 mL deionized water, then 1.6 g QA was added into the solution slowly under stirring at 25 °C for 48 h. After being purified by dialyzing in water for 4 days (MWCO 8000–14,000), the solution was lyophilized to give OQPGA light white powder.

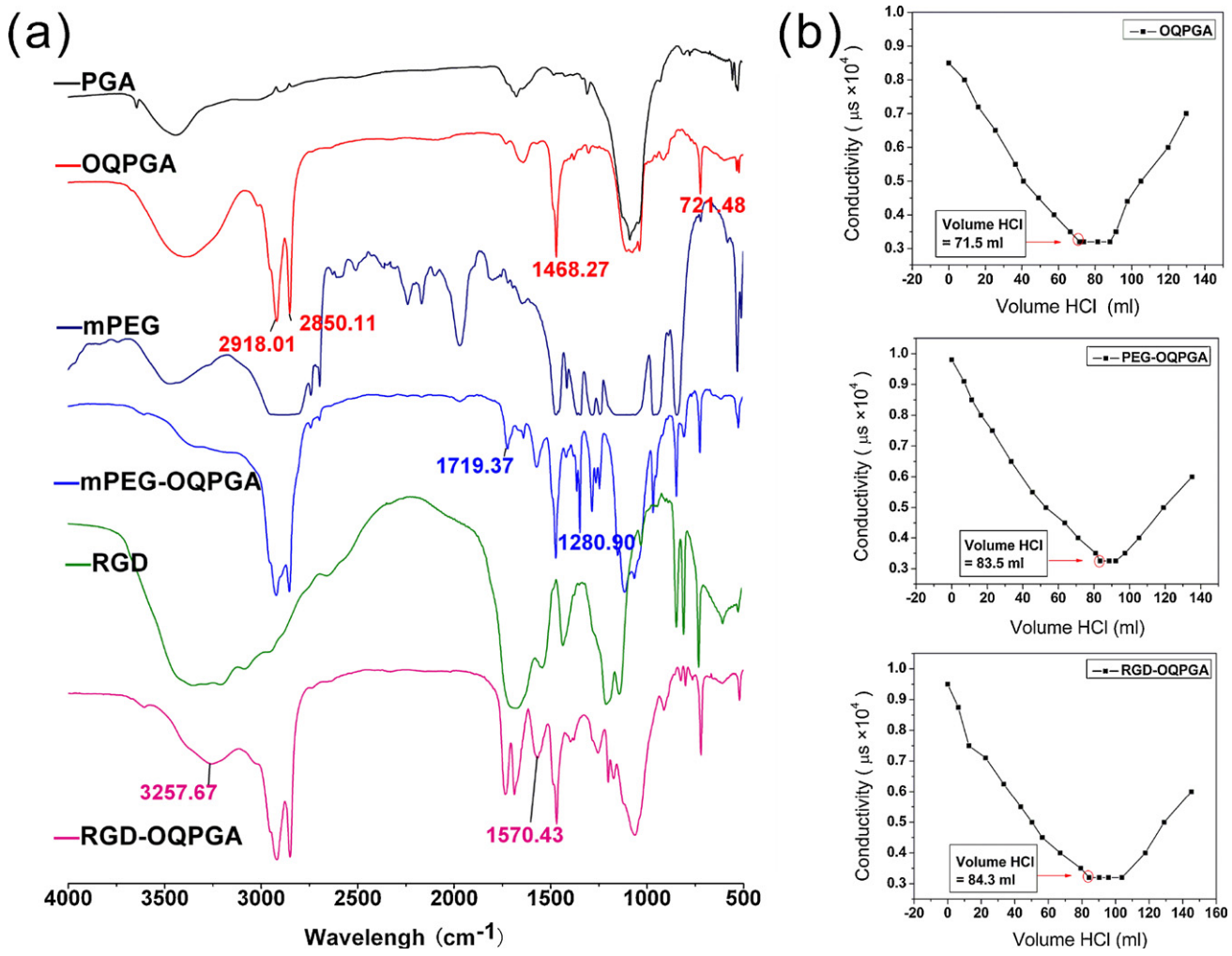

Fig. 2. (a) FT-IR spectra of PGA, OQPGA, PEG, mPEG-OQPGA, RGD, RGD-OQPGA.(b) The amount of carboxyl groups on OQPGA, mPEG-OQPGA and RGD-OQPGA were determined by conductometric titration.

The general preparation of PEG-OQPGA was shown in Fig. 1: 2 g mPEG was dissolved in 60 mL of chloroform, 20 mg hexamethylene diisocyanate (HMDI) were added into the solution slowly under stirring at 25 °C for 8 h. The chloroform was removed by vacuum with a rotary evaporator. The precipitate was separated out by aether. The excess HMDI was removed by dissolving in little chloroform, and then precipitate was separated out by adding aether. After vacuum drying, a white powder HMDI-mPEG was obtained. 500 mg HMDI-mPEG was dissolved in 60 mL chloroform, and 1 g OQPGA were added into suspension for 12 h reaction at room temperature under stirring. After being purified by dialyzing in water for 4 days (MWCO 8000–14,000), the solution was lyophilized to give PEG-OQPGA light white powder. The structures of OQPGA and PEG-OQPGA had been determined from FTIR spectra and ^{1}H NMR spectroscopy.

The general preparation of RGD-OQPGA according to the literature report (Zhang et al., 2010a,b) was shown as follows: 400 mg OQPGA was dissolved in 100 mL DCM, the solution was then stirred for 24 h under room temperature after adding EDC·HCl (100 mg) and NHS (85 mg). After evaporating the DCM, 10 mL of ACN was added to redissolve the polymer; 30 mg RGD peptide (dissolved in 50 mL PBS, pH 8.0) was added to solution and reacted for 24 h at room temperature. After being purified by dialyzing in water for 2 days (MWCO 8000–14,000), the solution was lyophilized to give RGD-OQPGA light white powder. The conjugation of RGD peptide to liposome was performed via coupling of the amine group on RGD peptide and the carboxyl group on OQPGA. The structure of RGD-OQPGA had been determined from FTIR spectra and ^{1}H NMR spectroscopy.

2.3. Physicochemical characterizations of OQPGA, PEG-OQPGA and RGD-OQPGA

The structures of OQPGA and its derivatives had been determined from FTIR spectra and ^{1}H NMR spectroscopy. FTIR spectra were recorded with KBr pellets on a Bio-Rad FTS 6000 spectrometer (Bio-Rad Company, Hercules, California, US) at room temperature. ^{1}H NMR spectra was recorded on a JEOLGX 400 D spectrometer operating at 400 MHz at room temperature.

The amount of carboxyl groups on polymers were determined by conductometric titration (Chen et al., 2002): 20 mg OQPGA, PEG-OQPGA, RGD-OQPGA were dissolved in 120 mL of 0.005 mol/L NaOH solutions, respectively. After 3 h magnetic stirring, 0.007 mol/L HCl (exact concentration were obtained by acid base titration) were added into the suspension gradually, observed conductivity variation as well.

Amphiphilic polymers with a suitable hydrophilic/hydrophobic balance can form a micellar structure when exposed to a selective solvent. The critical micelle concentration (CMC) was defined as the midpoint of the transition region before achieved micellar region. The OQPGA and its derivatives, consisting of hydrophilic PGA and hydrophobic long carbon segment, provided an opportunity to

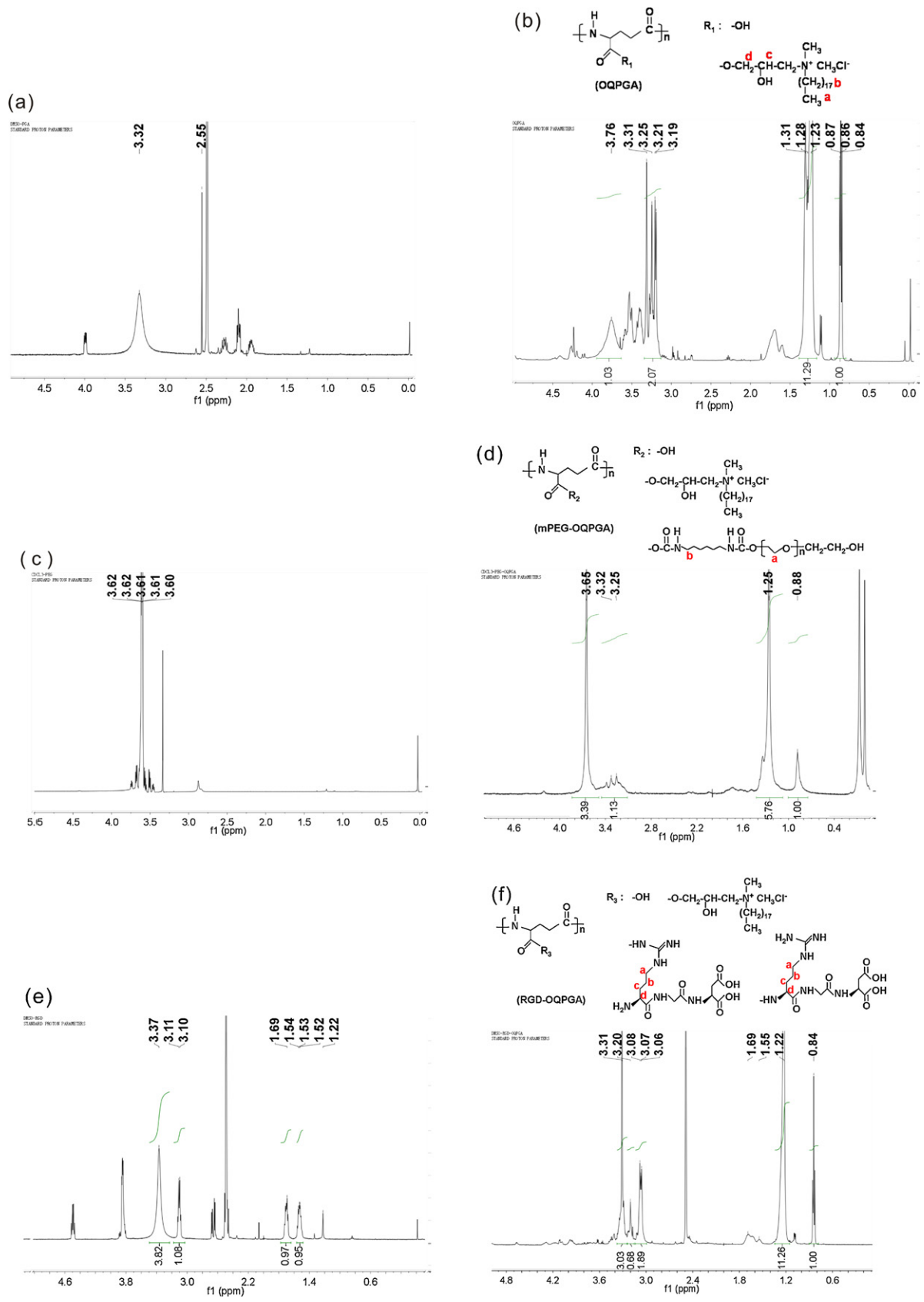

Fig. 3. ^{1}H NMR spectrum of (a) PGA, (b) OQPGA, (c) PEG, (d) mPEG-OQPGA, (e) RGD, and (f) RGD-OQPGA.

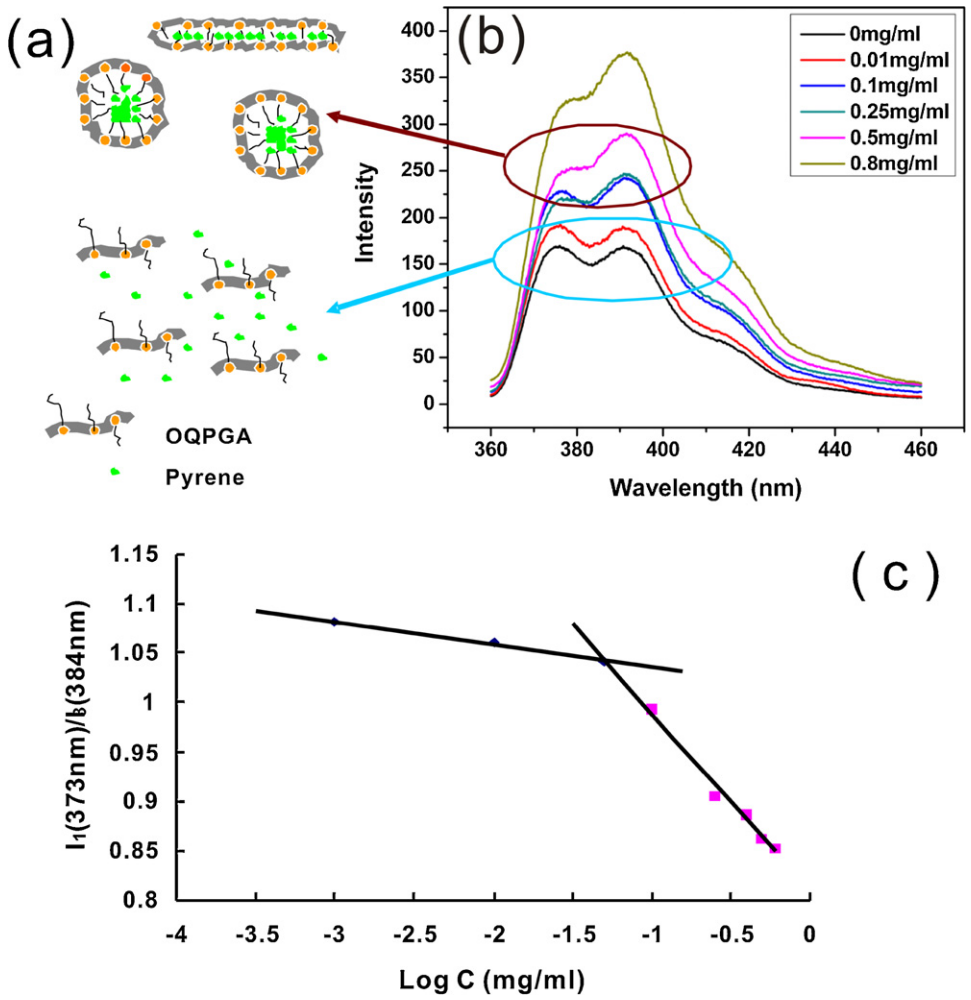

Fig. 4. (a) Schematic diagram of the behavior of pyrene in various concentrations of OQPGA. (b) The fluorescence emission spectra of pyrene were measured at various concentrations of OQPGA. (c) The ratio of fluorescence intensities at 373 and 384 nm (I373/I384) was plotted against the logarithm concentrations of OQPGA.

form micellar structure in water. The CMC of OQPGA was determined with a fluorescence spectrophotometer using pyrene as a fluorescence probe. The fluorescence excitation spectra of pyrene were measured at various concentrations of OQPGA from 0 to 0.8 mg/mL.

2.4. Samples preparation

PEG/RGD-MPLs preparation: PEG/RGD-MPLs were prepared by reverse-phase evaporation (REV) method as follows: OQPGA, PEG-OQPGA, RGD-OQPGA, Chol and Fe_3O_4 nanoparticles (weight ratio = 1:1:1:1.5:0.5, gross mass 30 mg) were dissolved in 4 mL DCM at room temperature under sonication for 2 min obtain organic phase. Then, 4 mL deionized water was mixed with organic phase under sonication for 300 s at 150 W output. The organic solvents were evaporated on a rotary evaporator to form PEG/RGD-MPLs suspension.

EPI load samples preparation: To evaluate nanoparticle stability and drug release profile of samples, two methods were used to prepare EPI loaded PEG/RGD-MPLs. PEG/RGD-MPLs-EPI 1 were prepared by film dispersion method as follows: OQPGA, PEG-OQPGA, RGD-OQPGA, Chol and Fe_3O_4 nanoparticles (weight ratio = 1:1:1:1.5:0.5, gross mass 30 mg) were dissolved in 4 mL DCM at room temperature under sonication for 2 min obtain organic phase. 3 mg EPI were dissolved in 4 mL deionized water to obtain aqueous phase. The organic solvents were evaporated on a rotary evaporator to form a thin film on the bottom of flask. Then, the dried film was dispersed by aqueous phase.

PEG/RGD-MPLs-EPI 2 were prepared by REV method, 3 mg EPI were dissolved in 4 mL deionized water to obtain aqueous phase. The other procedures were the same as previously (*PEG/RGD-MPLs preparation*). Simultaneously, MCLs-EPI (PEG-DSPE:Chol:EPI:Fe_3O_4 = 3:1.5:0.5:0.5), PEG-MPLs-EPI (OQPGA:PEG-OQPGA:Chol:EPI:Fe_3O_4 = 1.5:1.5:1.5:0.5:0.5) and PEG/RGD-PLs-EPI (PEG-OQPGA:RGD-OQPGA:Chol:EPI = 1.5:1.5:1.5:0.5) were also prepared by REV method according to *preparation of PEG/RGD-MPLs*.

2.5. Physicochemical characterizations of PEG/RGD-MPLs

The morphologies of the samples were observed via transmission electron microscopy (TEM). TEM observation of the microspheres was carried out at an operating voltage of 200 kV with a JEOL-100CXII in bright-field mode and by electron diffraction. Dilute suspensions of polymeric liposomes in water were dropped onto a carbon-coated copper grid by negatively staining with 2% phosphotungstic acid and then air dried.

The particle size and size distribution were determined by quasielastic laser light scattering with a Brookhaven Zetasizer (Brookhaven Instruments Ltd., US) at 25 °C. About 0.25 mL of each samples suspension was diluted with 2.5 mL of water immediately after preparation. Each experiment was repeated three times. The zeta potential was measured by using a Zetasizer (Brookhaven, US).

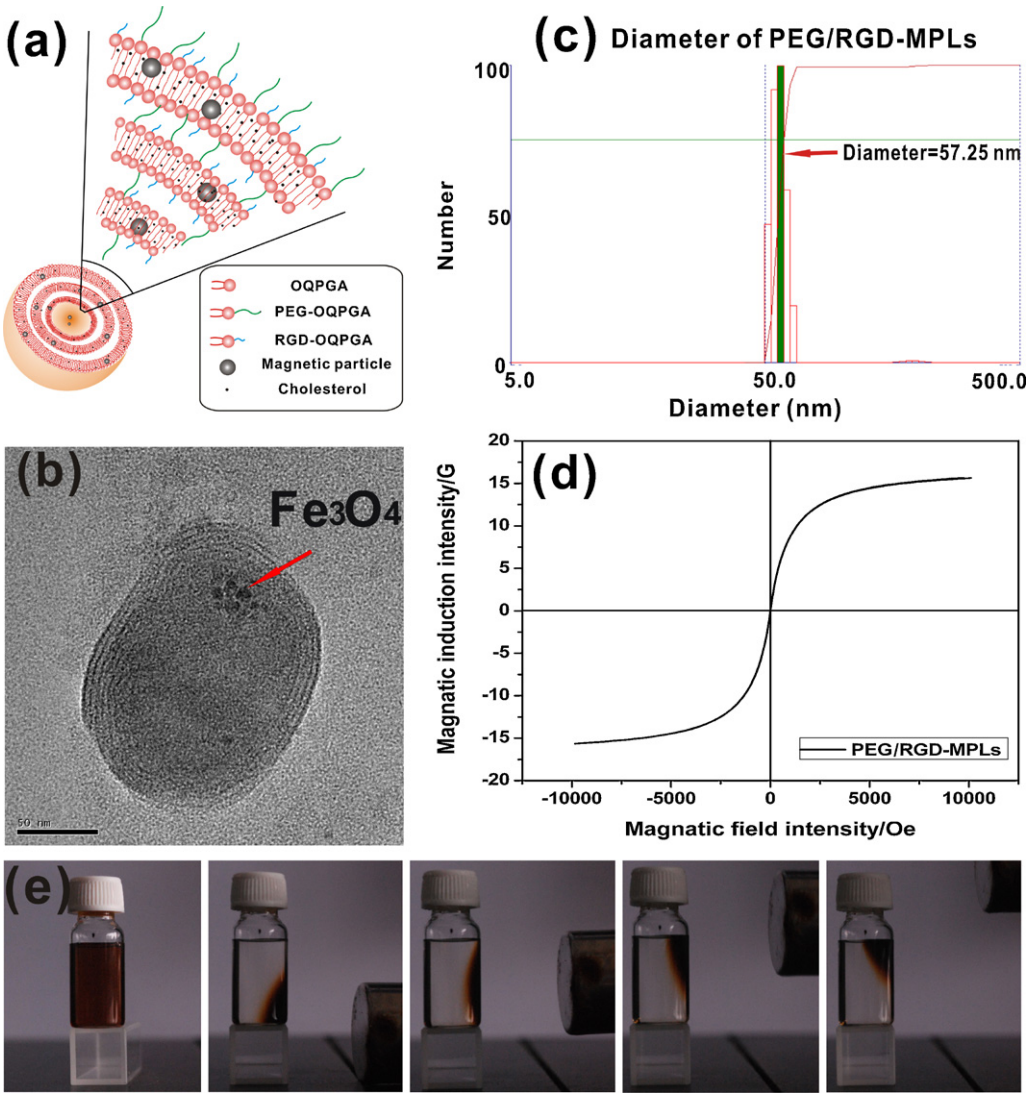

Fig. 5. (a) Schematic diagram of the structure of PEG/RGD-MPL. (b) TEM image of the PEG/RGD-MPL. (c) Particle size distribution of PEG/RGD-MPLs measured by DLS. (d) Magnetic hysteresis loop of PEG/RGD-MPLs. (e) The response of PEG/RGD-MPLs to the external magnetic field.

Zeta limits ranged from −150 to 150 V. Strobing parameters were set as follows: strobe delay −1.00, on time 200.00 ms, and off time 1.00 ms.

Magnetic measurement of sample was performed by a vibrating sample magnetometer (VSM) from LakeShore Ltd. The samples were in the form of powder and were placed in Teflon sample holder. The magnetic measurements (hysteresis loops) were carried out in the field region of $\pm T$ at room temperature.

To determine the drug loading efficiency (LE) and encapsulation efficiency (EE), a predetermined aliquot of EPI-loaded samples were first eluted through Sephadex G25 Column to remove any free EPI, respectively. The drug concentrations about free EPI were determined by UV spectrophotometer (JASCOV-570, Tokyo, Japan) at a fixed wavelength of 480 nm. The LE and EE of the samples were calculated from

$$\mathrm{LE}(\%) = \frac{A}{B} \times 100$$

$$\mathrm{EE}(\%) = \frac{C - D}{C} \times 100$$

where A was the weight of EPI encapsulated in liposomes, B was the weight of samples. C was the total amount of EPI, D was the amount of unencapsulated EPI.

To estimate the EPI release of the samples, the leakage of EPI from the samples were measured using UV spectrophotometer at wavelengths of 480 nm. When EPI was leaked out from the vesicles into the surrounding buffer, the absorbance increased dramatically. 3 mL of the sample suspensions was placed into a dialysis membrane bag (MWCO 8000–14,000), then placed into 8 mL Tris–HCl (pH = 7.4) buffer. The medium was kept at 37 °C under swing. After desired time, 3 mL solution was replaced with the same amount of fresh Tris–HCl (pH = 7.4). The absorbance of the EPI released from the samples was measured with a UV spectrophotometer at 480 nm. All measurements were performed in triplicate.

2.6. Cellular uptake studies

The cellular uptake of MCLs-EPI, PEG-MPLs-EPI, PEG/RGD-PLs-EPI, PEG/RGD-MPLs-EPI 2 were evaluated in MCF-7 cells by using an inverted Olympus microscope (IX-70) equipped with a digital color camera (Nikon D60), a broad-band ultraviolet (330–385 nm)

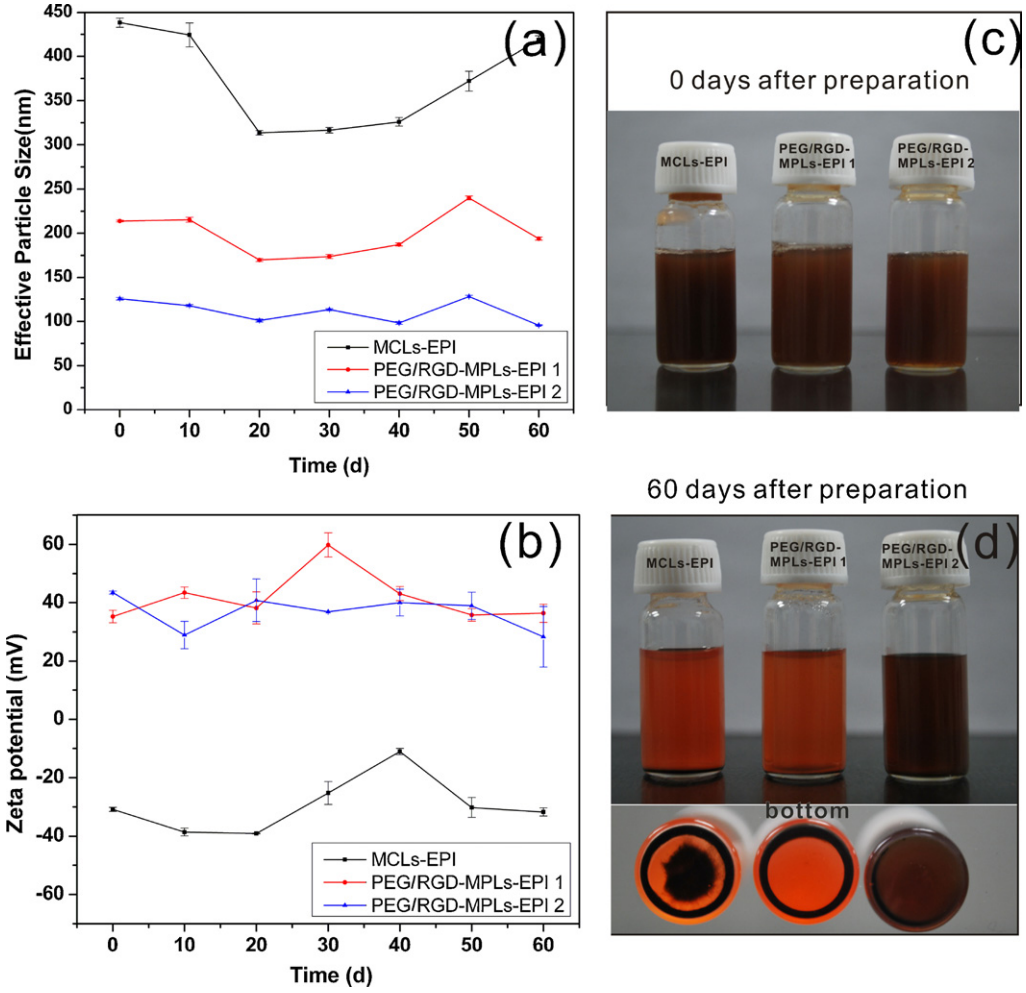

Fig. 6. (a) Effective particle size stability of samples. (b) Zeta potential stability of samples. (c) Photographs of samples after preparation and (d) photographs of samples on 60th days after preparation.

light source (100-W mercury lamp), and a long-pass interference filter (DM 400, Chroma Tech., Brattleboro, VT).

The cells were routinely grown at 37 °C with Dulbecco's modified essential medium (DMEM, Sigma D1152), supplemented with 10% fetal bovine serum (FBS). After 90% confluence, the cells were cultured in 24-well black plate at a density of 3×10^4 cells/well and grown overnight at 37 °C with 5% CO_2. Then, cells were incubated with suspension of EPI loaded MCLs, PEG-MPLs, PEG/RGD-PLs and PEG/RGD-MPLs with concentration 40 μg/mL for 0.5, 2.0 h, followed the media was removed and the cells were washed twice by cold PBS. Finally, the cells were taken to an inverted Olympus fluorescence microscope for imaging.

For magnetic induction of MCLs-EPI, PEG-MPLs-EPI, PEG/RGD-MPLs-EPI 2, a permanent magnet of strength 0.3 T was placed under the cell culture plate when samples were added in 24-well plate. The magnet was removed 10 min and the incubation continued for a total of 0.5 or 2 h. The following procedures were the same as previously described (Zheng et al., 2009).

2.7. Cytotoxicity assays

The cytotoxicity of the samples was evaluated using an MTT assay. GES-1 cells were seeded in DMEM supplemented with 10% FBS under 5% CO_2 at 37 °C. They were cultured in a 96-well plate in 100 μL medium per well at a density of 4000 cells/well for 24 h. Then cells were incubated with EPI and liposomal formulations under different concentrations at 37 °C for 48 h. 20 μL of 0.5 mg/mL MTT solution were added to each well and cells were incubated for another 4 h. The culture medium was subsequently discarded, and 200 μL of DMSO was added to dissolve the formazan crystals. Cell proliferation and viability were quantified spectrophotometrically by measuring the absorbance of the formazan product at the wavelength of 490 nm with a microplate reader (Model 680, Biorad). The data was expressed as the percentages of viable cells compared to the survival of a control group (untreated cells as controls of 100% viability).

3. Results and discussion

3.1. Structural characterization of OQPGA and its derivatives

The synthesis of OQPGA and its derivatives were shown in Fig. 1. The results of FT-IR analysis were shown in Fig. 2a. In the spectrum of OQPGA, the appearance of new intensive peak at 721.48 cm^{-1} ($n \geq 4$) corresponding to methylene planar rocking vibration which can be attributed to the long carbon segment of the quaternary ammonium salt (Qin et al., 2002). The two peaks at 2918.01 cm^{-1} (belongs to antisymmetrical stretching) and at 2850.11 cm^{-1} (belongs to symmetrical stretching) corresponded to methylene that also indicated the successful introduction of

quaternary ammonium salt. Meanwhile, the new characteristic peaks at 1468.27 cm^{-1} corresponded to bending vibration of C—H that derived from methylene. All of these indicated that the formation of OQPGA was synthesized successfully. In the spectrum of mPEG-OQPGA, the enhanced absorption peak at 1280.90 cm^{-1} (belongs to the C—N groups stretching of mPEG) and 1719.37 cm^{-1} (belongs to the C(=O)—O—C(=O) groups antisymmetric stretching) demonstrated that mPEG chains were successfully attached to OQPGA. In addition, the amount of carboxyl groups was determined by conductometric titration (Chen et al., 2002) and the results were shown in Fig. 2b. Measurements of conductometric titration have revealed that the content of carboxyl groups on OQPGA was 1.63 m mol/g, while that of PEG-OQPGA was 0.6 m mol/g. The reduction of carboxyl groups amount demonstrated that successful introduction of mPEG indirectly. The spectrum of RGD-OQPGA displays stretching vibration of NH_2 at 3257.67 cm^{-1}. The characteristic peak (1570.43 cm^{-1}) representing NH_2 symmetric bending that indicated that the presence of RGD peptide on the surface of OQPGA. The carboxyl groups amount of RGD-OQPGA were down from 1.63 m mol/g to 0.32 m mol/g also suggested that RGD peptide were successfully attached to OQPGA indirectly (Fig. 2b).

Typical ^1H NMR (DMSO or $CDCl_3$, δ; ppm) spectrum of samples were shown in Fig. 3, in the spectrum of OQPGA (Fig. 3b), the signal at δ 0.84–0.87, 3.19–3.31 and 3.76 were attributed to H-*a*, H-*c*, and H-*d*, respectively, which indicated that the QA were attached to PGA successfully. The most intensive signals at δ 1.23–1.31 corresponded to $-CH_2$ (H-*b*) which can be derived from the long carbon segment of QA. All of these confirmed that the formation of OQPGA was synthesized successfully. In the spectrum of mPEG-OQPGA (Fig. 3d), the most intensive signals at δ 3.65 were attributed to H-*a*, suggested that mPEG chains were successfully attached to OQPGA (Chan et al., 2007). The signals at δ 3.25–3.32 were corresponded to H-*b*, which also demonstrated that successful introduction of mPEG. As shown in the spectrum of RGD-OQPGA (Fig. 3f), the signals at δ 3.20–3.31, 1.55, 1.69, and 3.06–3.08 were attributed to H-*a*, H-*b*, H-*c* and H-*d*, respectively, which indicated successful attachment between RGD peptide and OQPGA.

3.2. Determination of critical micelle concentration (CMC)

Amphiphilic polymers consisting of hydrophilic and hydrophobic segments can self-assemble into micelle structures with the hydrophobic inner core and the hydrophilic outer shell in aqueous media (Wu et al., 2009). The CMC of OQPGA was determined with a fluorescence spectrophotometer using pyrene as a fluorescence probe (Cocera et al., 2001) (Fig. 4). Pyrene, as hydrophobic molecule, has a very low solubility in water and tends to solubilize itself into the hydrophobic region of nanoparticles (Fig. 4a). The fluorescence emission spectra of pyrene were measured at various concentrations of OQPGA from 0 to 0.8 mg/mL (Fig. 4b). The concentration of pyrene was kept at 6.0×10^{-7} M. The excitation wavelength was set at 338 nm and the intensities obtained from emission wavelengths at 373 and 384 nm were recorded. The ratio of fluorescence intensities at 373 and 384 nm (I373/I384) was calculated and plotted against the logarithm concentrations of OQPGA (Fig. 4c). The CMC was defined as the midpoint of the transition region before achieved micellar region. Markus Johnsson et al. have demonstrated that PEO-PPO-PEO tri-block copolymers with a CMC value of 0.1495 mg/mL constituted a stabilizing material for liposomes (Johnsson et al., 1999). As shown in Fig. 4c, the CMC values of OQPGA were determined as about 0.05 mg/mL. Those data suggested that amphiphilic OQPGA were easy to form nanoparticles self-assembly.

3.3. The morphology, particle size, zeta potential of PEG/RGD-MPLs

The TEM image in Fig. 5a showed that PEG/RGD-MPL was provided with a near-spherical shape. Obviously, the PEG/RGD-MPLs were multilamellar vesicle similar to CLs; meanwhile, Fe_3O_4 nanoparticles were encapsulated in vesicle successfully. A schematic illustration for the structure of PEG/RGD-MPL was presented in Fig. 5b. Due to the existence of the hydrophilic and the hydrophobic lipid bilayers, liposomes can accommodate both hydrophilic and hydrophobic molecule such as drugs, protein, antibody, etc. Besides, Fig. 5c showed that particle size of the PEG/RGD-MPLs was about 60 nm in large. Properties of drug carrier varied with particle characteristics, such as size and surface charge. For examples, compared to larger nanocarriers, smaller particle size (<200 nm) will tend to lower level of RES uptake, improve utilization ratio of drug and diminish drug side effects (Nishiyama and Kataoka, 2006).

3.4. Magnetic characterization of PEG/RGD-MPLs

The superparamagnetic colloids have emerged as a promising class of effective material in the targeting of delivery system. The ability of eliminating harm on normal cells and reducing the dosage required was relevant to whether the drugs can be transported to a specific site effectively. After magnetic carriers containing therapeutic drugs were injected into the circulatory system, a strong local magnetic field was applied to guide their accumulation in target tissues. The response speed of PEG/RGD-MPLs to the external magnetic field was determined by the magnetization saturation values. As shown in Fig. 5d, the magnetic hysteresis loop of PEG/RGD-MPLs was measured by using VSM. It was seen that PEG/RGD-MPLs sample with 15.5 emu/g magnetization still remain superparamagnetic and no residual magnetism. Importantly, the

Samples	LE (%)	EE (%)
MCLs-EPI	5.98%	74.35%
PEG/RGD-MPLs-EPI 1	7.54%	86.28%
PEG/RGD-MPLs-EPI 2	7.57%	86.52%

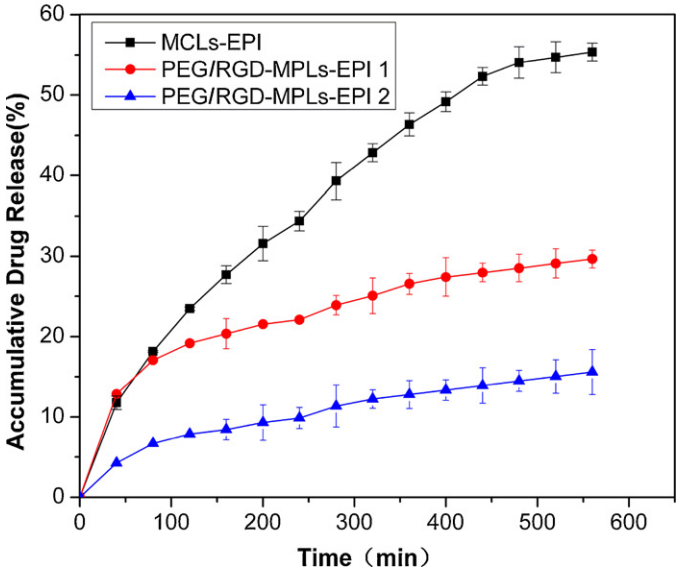

Fig. 7. (Top) The LE and EE of the samples. (Bottom) In vitro EPI release profile from the samples within 560 min for studying on the release effect.

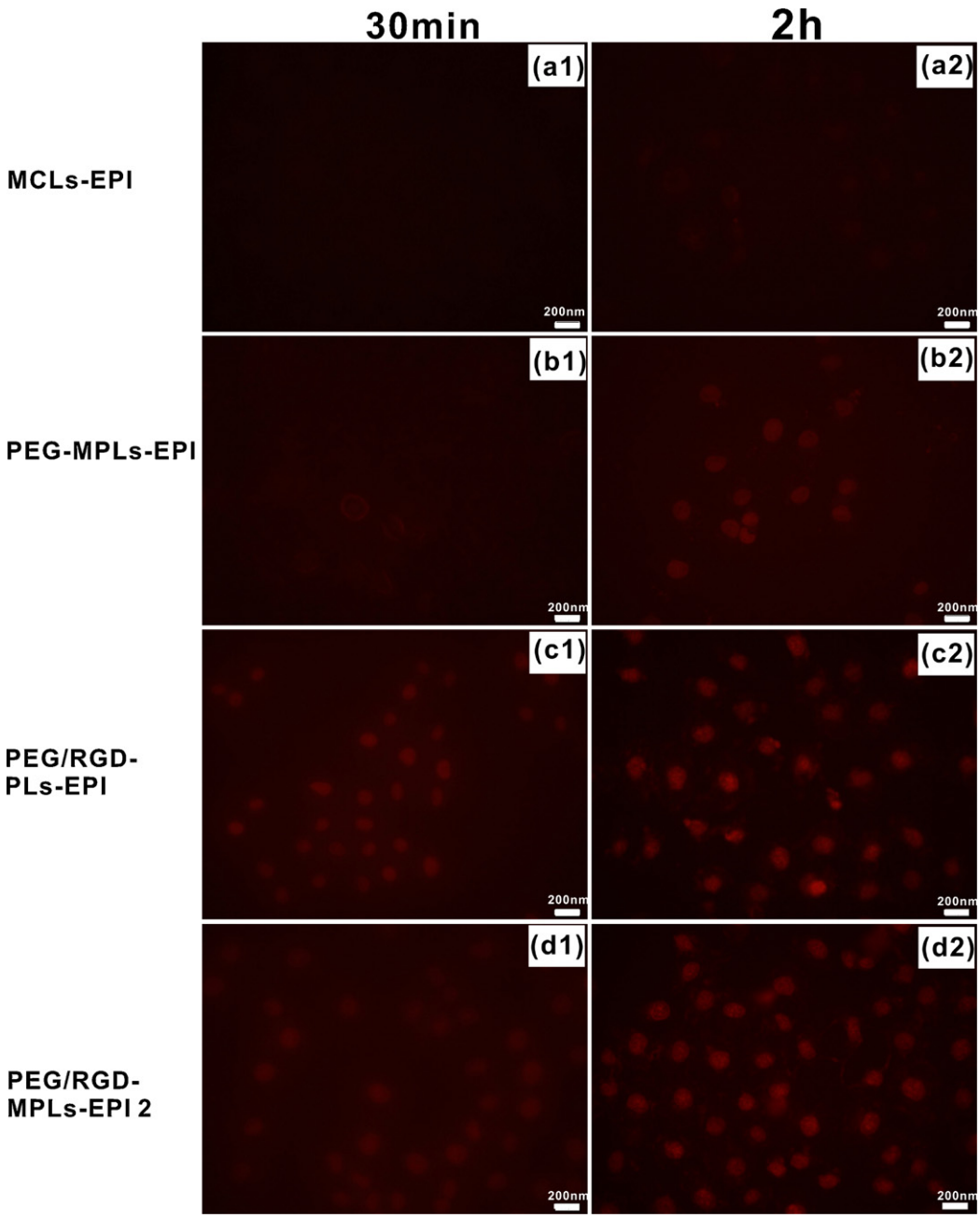

Fig. 8. (Left) Fluorescence microscopy images of MCF-7 cells incubated with samples after 30 min: (a1) MCLs-EPI, (b1) PEG-MPLs-EPI, (c1) PEG/RGD-PLs-EPI, and (d1) PEG/RGD-MPLs-EPI 2. (Right) Fluorescence microscopy images of MCF-7 cells incubated with samples after 2 h: (a2) MCLs-EPI, (b2) PEG-MPLs-EPI, (c2) PEG/RGD-PLs-EPI, and (d2) PEG/RGD-MPLs-EPI 2. Stronger emission indicates a higher level of EPI delivery. For magnetic induction of MCLs-EPI, PEG-MPLs-EPI, PEG/RGD-MPLs-EPI 2, a permanent magnet of strength 0.3 T was placed under the cell culture plate when samples were added in 24-well plate. The magnet was removed 10 min and the incubation continued for a total of 0.5 or 2 h.

PEG/RGD-MPLs with homogenous dispersion show sufficient response to the external magnetic field (Fig. 5e). It provided a possibility to responded to external permanent magnet with superparamagnetic characteristics, when was used for magnetic tissue targeting in vivo.

3.5. The stability of samples

To estimate the stability of samples at room temperature, we examined the size stability, zeta stability and Fe_3O_4 magnetic nanoparticles leakage behavior of EPI load MCLs, PEG/RGD-MPLs 1 and 2 (PEG/RGD-MPLs-EPI 1 and 2 represented EPI load PEG/RGD-MPLs prepared by film dispersion method and REV method, respectively). Fig. 6 shows size, zeta changes profiles and magnetic nanoparticles leakage profiles at room temperature. As shown in Fig. 6a, the size of MCLs-EPI decreased obviously from 440 nm to 328 nm after 20 days and increased to 420 nm on the 60th days. Conversely, the effective diameters of PEG/RGD-MPLs-EPI 1 were 175–220 nm and it changed slightly with respect to time. On the other hand, smaller particle size of PEG/RGD-MPLs-EPI 2 (100–120 nm) was observed and also no significant change with the time. All of this demonstrated that PEG/RGD-MPLs-EPI 1 and 2 were more stable than MCLs-EPI in size.

As shown in Fig. 6b, the zeta potentials of MCLs-EPI were −11 to −40 mV and changed significantly with time while that of PEG/RGD-MPLs-EPI 2 (28–40 mV) changed slightly at 60 days

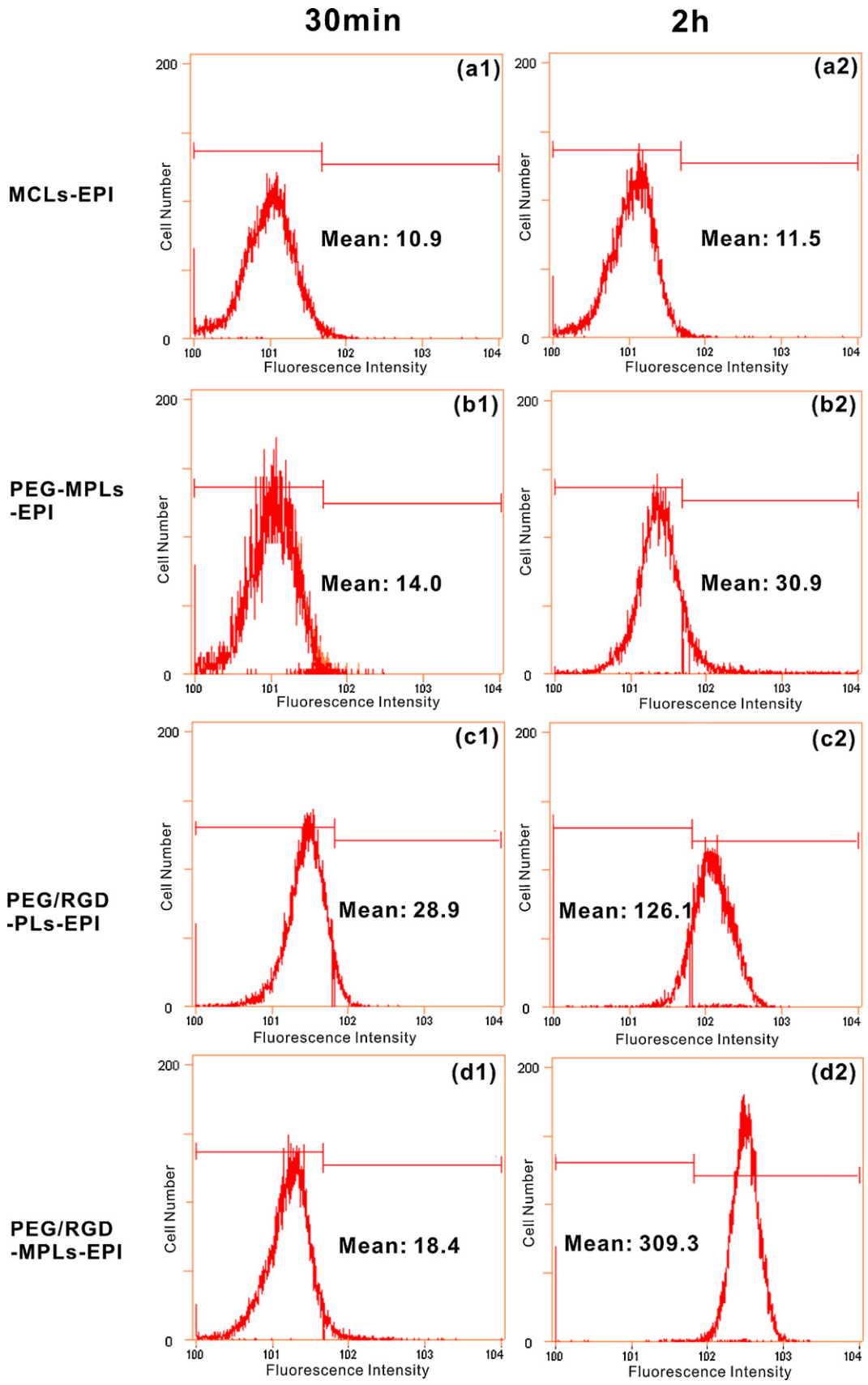

Fig. 9. (Left) Flow-cytometry histograms profiles of MCF-7 cells incubated with samples after 30 min: (a1) MCLs-EPI, (b1) PEG-MPLs-EPI, (c1) PEG/RGD-PLs-EPI, and (d1) PEG/RGD-MPLs-EPI 2. (Right) Flow-cytometry histograms of MCF-7 cells incubated with samples after 2 h: (a2) MCLs-EPI, (b2) PEG-MPLs-EPI, (c2) PEG/RGD-PLs-EPI, and (d2) PEG/RGD-MPLs-EPI 2. Higher intensity along the *x* axis (FL1) indicates more EPI delivery. "Mean" represents the mean fluorescence of cells.

after prepared. The negative charge on the MCLs-EPI surface may lead to low drug delivery efficiency because it was repelled by the negatively charged cell surface (Kostarelos and Miller, 2005).

To evaluate the Fe_3O_4 magnetic nanoparticles leakage behavior, we photographed samples after 60 days. As shown in Fig. 6d, PEG/RGD-MPLs-EPI 2 almost maintained homogeneous and produced little magnetic nanoparticles leakage compared with the other two samples on 60th days. The reason may be related to the fact that PEG/RGD-MPLs-EPI 2 prepared by reverse-phase evaporation method exhibited uniform particle size and stabilized zeta potential, which prevented aggregation and fusion itself. In other words, the PLs coated on magnetic nanoparticles formed an effective protective barrier to prevent nanoparticles leakage. Maybe its a useful magnetic delivery with sufficient stability to realize magnetic targeting in vivo.

3.6. EPI release from samples

The LE and EE of samples were shown in Fig. 7, compared to MCLs-EPI, PEG/RGD-MPLs-EPI 1 and 2 showed higher LE and EE. There was no significant change in LE and EE between PEG/RGD-MPLs-EPI 1 and 2. The drug release profile has been investigated by many methods: such as side-by-side diffusion cells with artificial biological membranes, dialysis bag diffusion technique, centrifugal ultrafiltration technique, and so on (Soppimath et al., 2001; Washington, 1990). In this work, the drug release profile was determined by dialysis method. The in vitro release behavior of EPI loaded MCLs, PEG/RGD-MPLs-EPI 1 and 2 were summarized in the cumulative percentage release shown in Fig. 7. The MCLs exhibited over 55% release of EPI after 560 min, with nearly 12.5% release occurring within 40 min. Conversely, PEG/RGD-MPLs-EPI 1 produced only 25% release after 24 h, with approximately 13% leakage occurring within the first 40 min which indicated that the controlled release of EPI from PEG/RGD-MPLs-EPI 1 was better than that from MCLs-EPI in Tris–HCl (pH = 7.4). The reason may be related to the fact that MCLs generally regarded as unstable capsules can be easily aggregated, fused, and leaked drug. But Compare with two samples, PEG/RGD-MPLs-EPI 2 (exhibited 9% release within the first 40 min, and approximately 13% leakage after 560 min) showed slow burst release and a longer release time.

3.7. Cellular uptake studies

The cellular uptake process of EPI-loaded MCLs, PEG-MPLs, PEG/RGD-PLs and PEG/RGD-MPLs into MCF-7 cells were assayed by fluorescence microscopy and flow cytometry (Figs. 8 and 9). The fluorescence images of the MCLs-EPI showed no fluorescence at the time point of 30 min (Fig. 8a1) and the negligible red fluorescence were obtained after incubation for 2 h (Fig. 8a2). These results were in line with flow cytometry studies (Fig. 9a1 and a2). The scarcer fluorescence in cells attributed to negative surface charge of MCLs-EPI, which can be easily repelled by the negatively charged cells surface. Compared to MCLs-EPI, PEG/MPLs-EPI showed a little red fluorescence after incubation for 30 min (Fig. 8b1) and the fluorescence intensity not only became stronger but also accumulated in cell nucleus after incubation for 2 h (Fig. 8b2). These maybe attributed to the fact that PEG-MPLs-EPI with positive charge easily incepted by cells. As described in Fig. 8c1 and c2, PEG/RGD-PLs-EPI showed fast cellular uptake, evidenced by red fluorescence was detectable in cells after incubation for 30 min. This was also confirmed by flow cytometry studies (Fig. 9c1 and c2). These data indicated that the presence of RGD peptide on the PLs surface could facilitate the transport of PLs into the nucleus (Auernheimer et al., 2005). Compared Fig. 8c1 with d1, non magnetic carriers (PEG/RGD-PLs-EPI) showed faster cellular uptake than magnetic carriers (PEG/RGD-MPLs-EPI) in short time, the reason maybe that PEG/RGD-PLs-EPI with smaller particles size (50–60 nm) were easier access to the cells. But magnetic carriers can guide accumulation on the surface of cells mostly with external magnetic fields, prompting more opportunities of cellular uptake by RGD targeting. As shown in Fig. 8d2, the image of the PEG/RGD-MPLs-EPI 2 showed stronger fluorescence intensities after 2 h incubation, which was also confirmed by flow cytometry studies (Fig. 9d2). All these data initially proved that RGD peptide and magnetic nanoparticles were helpful to transport nanocarrier into the cells and increased the feasibility of tumor targeting test in vivo.

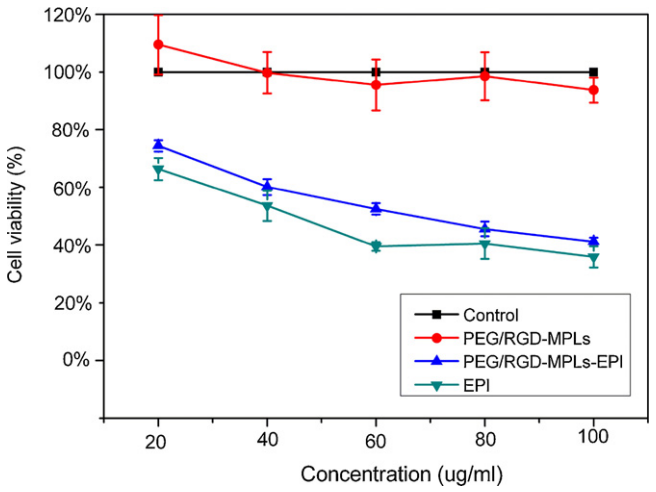

Fig. 10. Cell viability assay of GES-1 cells line after 48 h incubation with EPI, PEG/RGD-MPLs and EPI load PEG/RGD-MPLs. The results are expressed as the percentage compared to untreated cells. Each value represents the mean ± S.D. of three independent experiments.

3.8. Cytotoxicity assays

GES-1 cell line was selected to evaluate cellular cytotoxicity of the samples. The concentration of PEG/RGD-MPLs and PEG/RGD-MPLs-EPI ranged from 20 to 100 μg/mL, while EPI samples were at the same EPI concentration with PEG/RGD-MPLs-EPI. As shown in Fig. 10, the cell killing effect of EPI, PEG/RGD-MPLs and PEG/RGD-MPLs-EPI formulations were all concentration dependent. It was found that with increasing samples concentration, the cell viability decreased (or equivalently). The MTT analyses demonstrated that PEG/RGD-MPLs did not cause significant cytotoxicity against the cell line under the concentration of 100 μg/mL, suggesting low in vitro cytotoxicity to normal cells at ≤100 μg/mL. Under the same EPI concentration, PEG/RGD-MPLs-EPI showed lower cytotoxicity to normal cells than EPI samples, probably owing to effective tumor targeting by RGD and magnetic nanoparticles. This also meant that the PEG/RGD-MPLs were helpful to delivery more drug into the tumor cells and decreased damage to normal cells.

4. Conclusion

In this paper, new amphiphilic OQPGA, PEG-OQPGA, RGD-OQPGA were synthesized and their carboxyl groups amounts were measured. Self-assembled PEG/RGD-MPLs carriers were produced successfully. Compared to MCLs, PEG/RGD-MPLs exhibited sufficient size and zeta stability, controlled drug release and less magnetic nanoparticles leakage. The cellular uptake results suggested that the PEG/RGD-MPLs (with RGD and magnetic particles) exhibited more uptake than non RGD and non magnetism carriers in MCF-7 cells. MTT assay revealed that PEG/RGD-MPLs showed lower in vitro cytotoxicity to GES-1 cells at ≤100 μg/mL. These results showed that PEG/RGD-MPLs represented a promising

potential as an alternative multifunctional effective drug delivery system.

Acknowledgments

The authors gratefully acknowledge National Natural Science Foundation of China (50873076), National High Technology Program of China (863 Program) (2007AA021808), National High Technology Program of China (863 Program) (2007AA021802) and Tianjin Science and Technology Program (09ZCGYSF00900).

Appendix A. Supplementary data

Supplementary data assciated with this article can be found, in the online version, at doi:10.1016/j.ijpharm.2012.01.013.

References

Allen, Hansen, T.M., Martin, C., Redemann, F., Yau-Young., C., 1991. A Liposomes containing synthetic lipid derivatives of poly (ethylene glycol) show prolonged circulation half-lives in vivo. Biochim. Biophys. Acta 1066, 29–36.

Auernheimer, J., Dahmen, C., Hersel, U., Bausch, A., Kessler, H., 2005. Photoswitched cell adhesion on surfaces with RGD peptides. J. Am. Chem. Soc. 127, 16107–16110.

Benyettou, F., Lalatonne, Y., Sainte-Catherine, O., Monteil, M., Motte, L., 2009. Superparamagnetic nanovector with anti-cancer properties: gamma Fe_2O_3@Zoledronate. Int. J. Pharm. 379, 324–327.

Blank, W.J., He, Z.A., Picci, M., 2002. Catalysis of the epoxy–carboxyl reaction. J. Coat. Technol. 74, 33–41.

Blume, G., Cevc, G., 1990. Liposomes for the sustained drug release in vivo. Biochim. Biophys. Acta 1029, 91–97.

Chan, P., Kurisawa, M., Chung, J.E., Yang, Y.Y., 2007. Synthesis and characterization of chitosan-g-poly(ethylene glycol)-folate as a non-viral carrier for tumor-targeted gene delivery. Biomaterials 28, 540–549.

Chen, X., Cui, Z., Chen, Z., Zhang, K., Lu, G., Zhang, G., 2002. The synthesis and characterizations of monodisperse cross-linked polymer microspheres with carboxyl on the surface. Polymer 43, 4147–4152.

Cocera, M., Lopez, O., Coderch, L., Parra, J.L., de la, Maza.A., 2001. Solubilization of stratum corneum lipid liposomes by Triton X-100. Influence of the level of cholesteryl sulfate in the process. Colloids Surf. A: Physiochem. Eng. Aspects 182, 15–23.

Gabizon, A., Dagan, A., Goren, D., Barenholz, Y., Fuks, Z., 1982. Liposomes as in vivo carriers of adriamycin: reduced cardiac uptake and preserved antitumor activity in mice. Cancer Res. 42, 4734–4739.

Hirao, K., Sugita, T., Kubo, T., Igarashi, K., Tanimoto, K., Murakami, T., Yasunaga, Y., Ochi, M., 2003. Targeted gene delivery to human osteosarcoma cells with magnetic cationic liposomes under a magnetic field. Int. J. Oncol. 22, 1065–1071.

Ito, A., Honda, H., Kobayashi, T., 2006. Cancer immunotherapy based on intracellular hyperthermia using magnetite nanoparticles: a novel concept of heat-controlled necrosis with heat shock protein expression. Cancer Immunol. Immunother. 55, 320–328.

Johnsson, M., Silvander, M., Karlsson, G., Edwards, K., 1999. Effect of PEO-PPO-PEO triblock copolymers on structure and stability of phosphatidylcholine liposomes. Langmuir 15, 6314–6325.

Klibanov, A.L., Maruyama, K., Torchilin, V.P., Huang, L., 1990. Amphipathic polyethyleneglycols effectively prolong the circulation time of liposomes. FEBS Lett. 268, 235–237.

Kostarelos, K., Miller, A.D., 2005. Synthetic, self-assembly ABCD nanoparticles, a structural paradigm for viable synthetic non-viral vectors. Chem. Soc. Rev. 34, 970–994.

Li, S.D., Huang, L., 2009. Nanoparticles evading the reticuloendothelial system: role of the supported bilayer. Biochim. Biophys. Acta: Biomembr. 1788, 2259–2266.

Liang, X.F., Wang, H.J., Luo, H., Tian, H., Zhang, B.B., Hao, L.J., Teng, J.I., Chang, J., 2008a. Characterization of novel multifunctional cationic polymeric liposomes formed from octadecyl quaternized carboxymethyl chitosan/cholesterol and drug encapsulation. Langmuir 24, 7147–7153.

Liang, X.F., Wang, H.J., Tian, H., Luo, H., Chang, J., 2008b. Syntheis, structure and properties of novel quaternized carboxymethyl chitosan with drug loading capacity. Acta Phys. Chim. Sin. 24, 223–229.

Lubbe, A.S., Alexiou, C., Bergemann, C., 2001. Clinical applications of magnetic drug targeting. J. Surg. Res. 95, 200–206.

Maeda, H., Wu, J., Sawa, T., Matsumura, Y., Hori, K., 2000. Tumor vascular permeability and the EPR effect in macromolecular therapeutics: a review. J. Control. Release 65, 271–284.

Maruyama, K., Yuda, T., Okamoto, A., Ishikura, C., Kojima, S., Iwatsuru, M., 1991. Effect of molecular weight in amphipathic polyethyleneglycol on prolonging the circulation time of large unilamellar liposomes. Chem. Pharm. Bull. 39, 1620–1622.

Nishiyama, N., Kataoka, K., 2006. Current state achievements, and future prospects of polymeric micelles as nanocarriers for drug and gene delivery. Pharmacol. Ther. 112, 630–648.

Park, E.K., Lee, S.B., Lee, Y.M., 2005. Preparation and characterization of methoxy poly (ethylene glycol)/poly(epsilon-caprolactone) amphiphilic block copolymeric nanospheres for tumor-specific folate-mediated targeting of anticancer drugs. Biomaterials 26, 1053–1061.

Prencipe, G., Tabakman, S.M., Welsher, K., Liu, Z., Goodwin, A., ndrew, P., Zhang, L., Henry, J., Dai, H.J., 2009. PEG branched polymer for functionalization of nanomaterials with ultralong blood circulation. J. Am. Chem. Soc. 131, 4783–4787.

Qin, C.Q., Xiao, L., Du, Y.M., Shi, X.W., Chen, J.W., 2002. A new cross-linked quaternized-chitosan resin as the support of borohydride reducing agent. React. Funct. Polym. 50, 165–171.

Ruoslahti, E., 1996. RGD and other recognition sequences for integrins. Annu. Rev. Cell. Dev. Biol. 12, 697–715.

Soppimath, K.S., Aminabhavi, T.M., Kulkarni, A.R., Rudzinski, W.E., 2001. Biodegradable polymeric nanoparticles as drug delivery devices. J. Control. Release 70, 1–20.

Sun, S., Zeng, H., 2002. Size-controlled synthesis of magnetite nanoparticles. J. Am. Chem. Soc. 124, 8204–8205.

Verheul, R.J., Amidi, M., der Wal, S., van Riet, v., Jiskoot, E., Hennink, W.W.E., 2008. Synthesis, characterization and in vitro biological properties of O-methyl free N,N,N-trimethylated chitosan. Biomaterials 29, 3642–3649.

Wang, H.J., Zhao, P.Q., Liang, X.F., Gong, X.Q., Song, T., Niu, R.F., Chang, J., 2010. Folate-PEG coated cationic modified chitosan – cholesterol liposomes for tumor-targeted drug delivery. Biomaterials 31, 4129–4138.

Washington, C., 1990. Drug release from microdisperse systems a critical review. A critical review. Int. J. Pharm. 58, 1–12.

Wu, Y., Li, M.J., Gao, H.X., 2009. Polymeric micelle composed of PLA and chitosan as a drug carrier. J. Polym. Res. 16, 11–18.

Xiong, X.B., Huang, Y., Lu, W.L., Zhang, X., Zhang, H., Nagai, T., Zhang, Q., 2005. Enhanced intracellular delivery and improved antitumor efficacy of doxorubicin by sterically stabilized liposomes modified with a synthetic RGD mimetic. J. Control. Release 107, 262–275.

Zhang, L.F., Granick, S., 2006. How to stabilize phospholipid liposomes (using nanoparticles). Nano Lett. 6, 694–698.

Zhang, Y.F., Wang, J.C., Bian, D.Y., Zhang, X., Zhang, Q., 2010a. Targeted delivery of RGD-modified liposomes encapsulating both combretastatin. Eur. J. Pharm. Biopharm. 74, 467–473.

Zhang, Z., Lai, Y.X., Yu, L., 2010b. Effects of immobilizing sites of RGD peptides in amphiphilic block copolymers on efficacy of cell adhesion. Biomaterials 31, 7873–7882.

Zheng, X., Lu, J., Deng, L., Yang, X., Chen, J., 2009. Preparation and characterization of magnetic cationic liposome in gene delivery. Int. J. Pharm. 366, 211–217.

Zhu, Y.F., Fang, Y., Kaskel, S., 2010. Folate-conjugated Fe_3O_4@SiO_2 hollow mesoporous spheres for targeted anticancer drug delivery. J. Phys. Chem. C 114, 16382–16388.